Letter

Efficient ion acceleration by multistaged intense short laser pulses

J. Kim,[1,*] S. Wilks,[2] A. Kemp,[2] M. Sherlock,[2] T. Ma,[2] F. Beg,[1] and D. Mariscal[2]
[1]*Center for Energy Research, University of California, San Diego, 92093 California, USA*
[2]*Lawrence Livermore National Laboratory, Livermore, 94550 California, USA*

(Received 6 October 2020; accepted 4 May 2022; published 6 July 2022)

We present a computational study of laser-driven ion acceleration that optimizes a combination of target transparency and extended field acceleration at moderate relativistic intensity. Our scheme applies two sequential laser pulses irradiating a thin target foil along the same direction: The first pulse drives a rapid expansion of the target, while the second one drives a quasistatic electric field in the expanding target with increasing electron temperature. In our particle-in-cell simulations we observe proton peak energies and numbers enhanced by factors of up to 3 compared with regular target-normal sheath acceleration.

DOI: 10.1103/PhysRevResearch.4.L032003

Ion acceleration driven by relativistic short-pulse lasers is an active research area as it provides strong current beams of tens of kiloamperes, i.e., four orders of magnitude more than what is found in conventional accelerators. These very bright ion beams are appealing for their potential to improve a broad range of applications that include neutron sources [1], exotic isotope creation [2], novel inertial confinement fusion (ICF) ignition schemes [3], proton therapy [4], isochoric heating sources [5], and high-fluence proton radiography [6]. For the laser-based approach to become widely adopted, increasing the maximum energy $E_{\max}$ of ions is required. The nominal approach for achieving this requirement is to use more intense laser pulses for various ion acceleration mechanisms such as target-normal sheath acceleration (TNSA) [7,8], the magnetic vortex [9], the breakout afterburner (BOA) [10,11], and radiation pressure acceleration (RPA) [12]. While effective, increasing the laser intensity is limited by the rate of technological progress and the cost of advanced lasers.

The TNSA mechanism, the most intensively investigated concept for laser-driven ion acceleration, has demonstrated higher maximum proton energy with increasing laser intensity [13]. This trend is described with well-known models [14] based on an isothermal assumption [15], where $E_{\max}$ is proportional to the hot-electron temperature T_{hot} given by the ponderomotive scaling [16], $T_{\text{hot}} \sim \sqrt{I\lambda^2}$, which predicts that higher laser intensity results in higher ion energy, which is in good agreement with a wide range of subpicosecond experimental data [17]. However, there exist clear limitations to enhancing the maximum ion energy due to the limited laser intensity ($<1 \times 10^{23}$ W/cm^2) that current facilities can provide.

On the other hand, recent studies using energetic multipicosecond pulses have shown promising results [17,18] suggesting a new approach to ion acceleration at modest laser intensities. Proton energies of up to 20 MeV at quasirelativistic intensities, $\sim 1 \times 10^{18}$ W/cm^2 [17], and ~40-MeV protons from a quasishaped pulse (double multipicosecond pulses) have been observed in recent experiments, which are far beyond the energies seen in prior experiments for the same laser intensity with subpicosecond pulses. Laser pulses interacting with an expanding underdense plasma for multipicosecond duration generate a "superponderomotive" electron population in addition to the usual ponderomotive spectrum [19]. This mechanism is the key to continuously sustaining electric fields for proton acceleration that results in a boost to the maximum proton energy.

Beyond TNSA, ion acceleration from laser-induced transparent plasmas is predicted to deliver advantages such as high yield and high ion energy. In this regime, an opaque thin solid-foil (submicrometer thick) or initially near-critical-density (NCD) target becomes transparent to the laser pulse due to electron heating and expansion. The physics behind ion acceleration in this regime include volumetric heating [20], the Buneman instability [10], the magnetic vortex [21], and a combination of TNSA and RPA mechanisms [22]. Recent studies in this regime utilized nanotube foam targets to enhance electron heating, resulting in enhancement of the maximum proton energy from 12 MeV to 30 MeV [23], and double laser pulses to help with the onset of BOA [24], where the first pulse, with an intensity of $\sim 10^{19}$ W/cm^2, acts as a prepulse, changing the target electron distribution to enhance the laser absorption for the main pulse interaction.

In this Research Letter, we present a scheme to enhance the peak cutoff energy and flux of short-pulse laser-accelerated ions via the synergetic effects of target transparency and continuous field acceleration. Here, in this computational study using the particle-in-cell (PIC) code EPOCH, instead of postulating future ultrahigh laser intensity values, we employ realistic laser parameters: moderate intensity ($1–8 \times 10^{20}$ W/cm^2), pulse duration of up to 1 ps.

*jok035@ucsd.edu

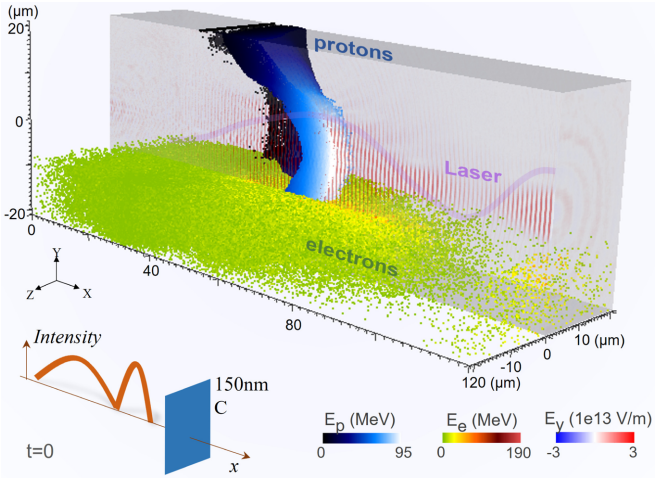

FIG. 1. Snapshot of 3D PIC simulation of ion acceleration at $t = 530$ fs. Two laser pulses (80 fs, 8×10^{20} W/cm^2 + 160 fs, 4×10^{20} W/cm^2) were sent consecutively to the carbon foil ($60n_c$, 150 nm thick), where a 20-nm-thick hydrogen layer is added to the rear surface. In the 3D result, the proton energy and laser electric field are presented in half of the box (right side, $Z > 0$), and electron energy is shown in the bottom quarter ($Y < -10$ μm).

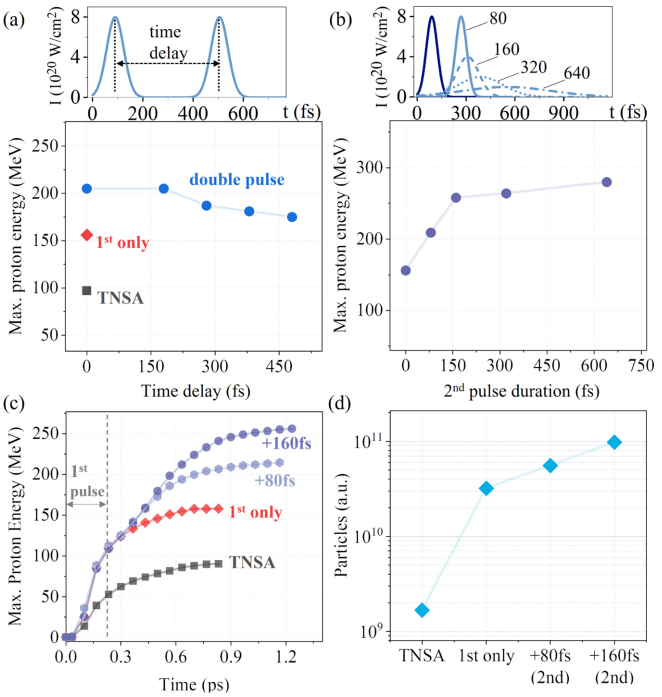

FIG. 2. Maximum proton energies from different pulse combinations in simulations with 2D Cartesian coordinates. (a) Two pulses (80 fs duration each) with different time delays compared with the single-pulse case. (b) A first pulse (80 fs duration) followed by a second pulse with duration 80, 160, 320, or 640 fs at fixed pulse energy. (c) Time evolution of peak proton energy in the cases from (a) and (b). (d) Accelerated proton numbers (>80 MeV).

Figure 1 shows a map of protons, electrons, and the laser field from a three-dimensional (3D) simulation presenting a signature of the acceleration scheme investigated in this Research Letter. Initially, a 150-nm-thick carbon target with an electron density of $60n_c$ is heated by the first laser pulse and expands, allowing a second pulse to penetrate the target debris. The continuous interaction of this second pulse with the expanding plasma generates copious hot electrons that help to accelerate protons and carbon ions.

In the case of typical TNSA, hot electrons generated from the target expand in both transverse and longitudinal directions, and their density quickly drops. Moreover, since the hot-electron source is at the target front side, the supply of hot electrons that can reach the proton beam front is geometrically limited by hot-electron-cloud expansion. In our scheme, the main part of the laser can penetrate the transparent target that transitioned from opaque to an expanding plasma with a large-scale underdense plasma during the long (second) pulse duration, continuously generating energetic electrons. Now that the electron source is volumetric in nature and closer to the location of the most energetic ions, more electrons can reach the ion beam front, and a strong, comoving electric field further accelerates ions.

To understand the underlying physics behind the acceleration, we have performed a systematic computational study with various laser pulse parameters using 2D PIC simulations. In the simulations, a spatial resolution of 100×50 cells (in x and y) per laser wavelength (=1 μm) is used, and numerical convergence was checked with a finer resolution.

Figure 2 presents a comparison of protons from various pulse combinations in the simulations. Firstly, the maximum proton energies from two pulses (8×10^{20} W/cm^2 and 80 fs duration each) with different time delays between the two are compared as shown in Fig. 2(a). Except for the TNSA case, targets used in all cases are initially $60n_c$ (electron density), 150-nm-thick carbon foils with a hydrogen layer appended at the back surface. With a greater initial density than critical density for a given laser intensity, $n_{e0} > \gamma n_c \sim a/\sqrt{2}n_c \sim 17n_c$, and thicker than skin depth, $L_0 > \sqrt{\gamma}c/w_p \sim 80$ nm, the target is initially opaque to the laser. Here, γ and a are the Lorentz factor and the normalized laser amplitude, respectively. However, an 80 fs pulse duration is long enough to allow the target to become relativistically transparent, as a transit time can be estimated with a 1D model [20] as $\tau > L_0/2C_s(\sqrt{2}n_{e0}/a_0n_c) \sim 20$ fs. L_0 and w_p are the initial target thickness and the plasma frequency, respectively. Consistent with previous work [20], protons accelerated from a relativistic transparency regime have higher maximum energy than TNSA [see red diamond and black square in Fig. 2(a)]. Here, the TNSA case is represented by a single pulse with energy such that its peak intensity (1.6×10^{21} W/cm^2) is even higher than the double-pulse cases. The target, initially with solid density, $\sim 10^{24}$ cm^{-3}, for this case, remains opaque resulting in typical TNSA without entering the transparency regime. TNSA efficiency is influenced by the prepulse and preplasma. In these simulations, preplasma gradients were not included at the front surfaces for the sake of comparison. The range of intensities is inevitably limited, but existing experimental facilities, e.g., the National Ignition Facility's Advanced Radiographic Capability (NIF-ARC), OMEGA Extended Performance (OMEGA EP), and Laser for Fast Ignition Experiment (LFEX), are capable of sending multiple laser pulses to a single target [25–27]. When

the two pulses have a relatively short time delay, 160 fs, for example, the maximum proton energy resulting from this case is equal to the maximum proton energy from a single pulse with doubled intensity (time delay = 0 in the plot). However, a longer time delay weakens the influence of the second pulse, resulting in a declining maximum proton energy that is eventually analogous to the one-pulse case. Use of a double pulse with a time delay between the two pulses can give an enhancement of the maximum proton energy: 210 MeV, up from the 150 MeV of a single pulse. Here, the proton energy of 210 MeV achieved from two pulses with 160-fs time gap is similar to what a single pulse with twice the intensity can generate. This shows the benefit of using two pulses when the ability to increase laser intensities is limited.

In the top panel of Fig. 2(b), the first pulse (80 fs duration) is fixed for all cases, and the following second pulse is given with a duration of 80, 160, 320, or 640 fs where the peak of the pulses moves back according to pulse length to avoid initial overlap of the two pulses. For a longer pulse duration, the laser intensity is reduced to keep the total laser energy the same. A notable result from this study is an enhancement in maximum proton energies with longer pulse durations despite the lower intensity. Compared with the matched double pulses (80 fs + 80 fs), which accelerate protons to ~210 MeV, the longest case (80 fs + 640 fs) results in higher energy, ~280 MeV. This aspect also emerges in the time evolution of maximum proton energies as shown in Fig. 2(c), where a pulse that is twice longer (160 fs) but has half the intensity leads to greater proton energy than the case of a single 80-fs pulse. The trend of these enhanced proton energies with a longer pulse duration has been demonstrated with 3D simulations, which show about 60–70% of maximum proton energies obtained in 2D. The difference between the 2D and 3D cases is mainly from inherently different dimensional effects where plasma expansion in 2D is marginally underestimated. Thus onset of target transparency time is earlier in 3D than 2D, and optimal target areal density for ion acceleration depends on the simulation dimension [28]. Note that with a single long pulse (multipicosecond), the target becomes transparent and field generation extends via continuous laser interaction somewhat similar to the way a double pulse behaves. However, for a given laser energy, precisely shaped pulses are preferred as the temporal profile since the intensity peaks can be chosen to optimize proton acceleration. As expected, increasing laser intensity for a relatively long pulse improves the maximum proton energy. Increasing the intensity by 2 and 3 times with a fixed duration of 640 fs [Fig. 2(b) case] accelerates protons up to 310 and 340 MeV, respectively.

A significant enhancement in accelerated ion numbers is one of the biggest advantages of the scheme presented in this Research Letter, in addition to an improved maximum ion energy. Figure 2(d) shows quantitatively how the proton numbers vary for each case. For example, the number of protons with energy greater than 80 MeV increases with pulse length by almost two orders of magnitude compared with TNSA. While ions produced from the TNSA mechanism typically have a sharply falling Maxwellian energy spectrum, acceleration via an additional laser pulse efficiently shifts a large ion population to higher energy. These substantial increases

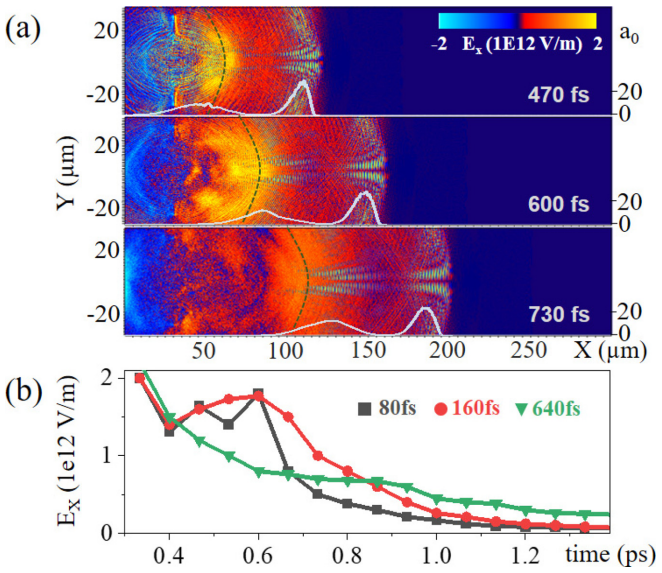

FIG. 3. (a) Electric fields in the longitudinal direction, E_x, in time for the case where the second-pulse duration is 160 fs. Dashed lines represent the proton beam front (fastest protons) at each time. Laser intensities, a_0, at $Y = 0$ for each time are shown with the white lines. (b) Time-dependent E_x measured at the proton beam front for different second-pulse durations: 80, 160, and 640 fs.

in energetic ion numbers are beneficial for applications that require a high fluence of ions.

In the double-pulse case, the additional ion acceleration is the consequence of the extended electric fields and increased potential near charge separation in the electron cloud driven by the second pulse. Figure 3(a) displays time-evolving electric fields, E_x, induced by the second pulse [the 80 fs + 160 fs case in Fig. 2(b)]. At each time, the electric field peaks (spatially in x) near the ion beam front which is shown with the dashed line in Fig. 3(a), indicating the charge separation (ions and electrons) in expanding plasmas. By the end of the second pulse of 160 fs, a strong electric field E_x on the order of 1×10^{12} V/m is maintained for up to 1 ps, which is a significantly longer duration than the single-pulse (80 fs) case, where E_x tends to quickly diminish in 200 fs. An even stronger E_x results for a longer pulse duration for the second pulse, as shown in Fig. 3(b), where initially weak but increasingly stronger fields are seen at later times; see the 320- and 640-fs cases after ~0.8 ps in Fig. 3(b).

Electric fields, the acceleration fields for ions, are strongly influenced by the evolution of the hot electrons in time. Figure 4 shows particle momentum and position for the double-pulse scheme. Firstly, electrons experience multistage energy gain and loss. As shown in Figs. 4(a) and 4(b), a small portion of the target electrons accelerate and move with the first pulse (80 fs) as the target starts becoming relativistically transparent, while a larger volume of electrons expands with the second, longer pulse (160 fs). Using particle tracking diagnostics, an example of electron energy history is exhibited in Fig. 4(c), where two stars indicate the electron position and time corresponding to Figs. 4(a) and 4(b). The electron continuously gains energy (~80 MeV) by the front part of the second pulse and suddenly loses energy when it crosses

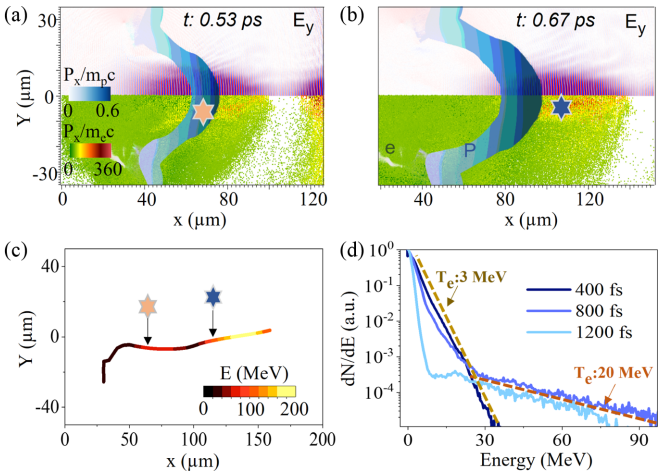

FIG. 4. Electrons accelerated by the double pulse (80 fs + 160 fs). (a) and (b) Laser field (upper half) and particle momentum P_x (bottom half) at 0.53 and 0.67 ps. Proton P_x is scaled with color (white to blue). The position of an example electron for the particle trajectory is marked with a star. (c) Electron trajectory with time history of its energy. (d) Electron energy spectra measured at 400, 800, and 1200 fs.

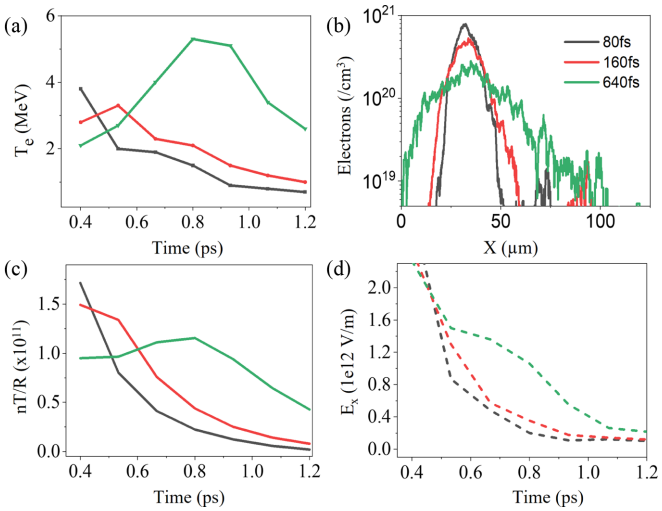

FIG. 5. Simulation results from 80 fs (first pulse) followed by different durations of the second pulse: 80, 160, and 640 fs are represented with black, red, and green, respectively [(a)–(d)]. (a) Measured electron temperatures. (b) Density of target electrons when the peak of the second pulse arrives at the initial target position. (c) Electron pressure over range of proton expansion. (d) Calculated electric sheath fields using time-varying hot-electron temperatures measured from simulations.

the proton beam front after 0.53 ps. This energy drop is due to energy coupling from electron to protons, which is the process of proton acceleration. Then, the electron gains energy again to a value over 100 MeV due to the interaction with the second pulse penetrating the transparent plasma. The energy distribution of the entire electron population is shown in Fig. 4(d). While electron distributions can be characterized by a single temperature at early times (400 fs), a two-temperature distribution is observed, with decreasing bulk temperature and increasing temperature for hot electrons, where the temperature of 3 MeV is slightly lower than ∼5.5 MeV, ponderomotive scaling, for the second pulse but the hot tail shows much higher temperature, 20 MeV. Here, as the energy history of tracked particle exhibits, hot tails of spectra are constructed when electrons expelled out of the proton beam front are reaccelerated by direct interaction with a laser pulse.

Figure 5 shows comparisons of electron temperature and electric fields from simulations using different durations of the second pulse (80, 160, and 640 fs). A comparison of electron temperatures is presented in Fig. 5(a). In the measurement of temperatures, first-pulse-driven hot (energetic) tails of the distribution are excluded, and only electrons near the proton beam front are counted. The effective electron temperature increases up to 5 MeV within 1 ps in the case of a 640-fs pulse, while electron temperature peaks to 3 MeV and quickly drops within 0.5 ps for the case of a 160-fs second pulse. Here, the electron temperature of ∼ 5 MeV for the 640-fs-pulse case is greater than electron temperatures predicted with ponderomotive temperature scaling [16], for a given pulse intensity, 1×10^{20} W/cm^2. The underlying physics here is that with longer pulse duration, the plasma (initially a thin foil) expands and develops a large-scale, underdense plasma where the laser-plasma interaction can generate superponderomotive electrons. The generation of superponderomotive electrons in near-critical or subcritical plasmas has recently been investigated via experiments [29], and numerical studies suggesting various mechanisms such as stochastic heating [30], direct laser acceleration with a channeling effect or longitudinal laser fields [31,32], and an electrostatic potential [33]. In general, longer pulses contain a proportionally greater fraction of energy in superponderomotive electrons than shorter (<100 fs) pulses. The expanded electron densities for each of the double-pulse cases are compared in Fig. 5(b).

In addition, one physical feature in these cases is that the laser pulse propagating in larger-scale underdense plasma with longer pulse duration can be self-focused by spatially varying the index of refraction of the plasma. For example, in Fig. 3(a), the intensity of the longer, second pulse (indicated as a white line with the preceding first pulse) increases with time as it propagates through the expanding plasma. An increase in laser intensity, due to this focusing effect, also works positively for boosting electron temperature [23].

To validate the electron contribution to the accelerating electric field for ions, the energy density of electrons over the range of ion expansion, nT/R, where R is the distance of plasma expansion (from initial target rear surface to proton beam front) during time t, is calculated using measured values as shown in Fig. 5(c). Additionally, in Fig. 5(d), the electric sheath field with a time-dependent electron temperature in the expanding plasma is calculated by using the theoretical 1D model, $E_f = 2\frac{T_e}{eR}\Theta$, $\Theta = 1 + (R\ddot{R}/\dot{R}^2)/2$ [34]. From Fig. 5(d), a stronger electric field is observed for a longer period of time with longer laser pulse duration. Moreover, these results are qualitatively similar to the fields observed in the simulation; see Fig. 3(b).

In summary, we have shown in parametric studies of 2D and 3D PIC simulations how a combination of staged multiple

laser pulses on thin solid targets can yield a significant enhancement of the maximum proton energy via the synergetic effects of target transparency and continuous field acceleration. In addition, the presented scheme shows a high flux of ions for high energy as it efficiently shifts a large ion population to higher energy. Double pulses with a certain time delay between the two pulses can increase the maximum proton energy to the energy that can be achieved with a single pulse of twice the laser intensity. Thus this shows the potential benefit of using two pulses as the ability to increase laser intensities is limited due to the inherent threshold of optical elements to avoid damage in most laser facilities. Beyond this result, the maximum proton energy can be further improved by using a longer pulse duration for the second pulse. Even second pulses with relatively low intensity and longer duration (1×10^{20} W/cm^2, 640 fs) can interact with largely developed underdense plasma, resulting in energetic hot electrons in the superponderomotive regime. The increase in electron temperature leads to maximum proton energy enhancements compared with a typical proton acceleration with TNSA for a given laser intensity.

This work was funded under the auspices of the US Department of Energy by Lawrence Livermore National Laboratory under Contract No. DE-AC5207NA27344 with funding support from the Laboratory Directed Research and Development Program under Tracking Codes No. 17-ERD-039 and No. 20-ERD-048, and DOE Office of Science Early Career Research Program under SCW1651. This document was prepared as an account of work sponsored by an agency of the U.S. Government. Neither the U.S. Government nor Lawrence Livermore National Security, LLC, nor any of their employees makes any warranty, expressed or implied, or assumes any legal liability or responsibility for the accuracy, completeness, or usefulness of any information, apparatus, product, or process disclosed, or represents that its use would not infringe privately owned rights. The views and opinions of authors expressed herein do not necessarily state or reflect those of the U.S. Government or Lawrence Livermore National Security, LLC, and shall not be used for advertising or product endorsement purposes. The PIC code EPOCH was funded by UK EPSRC Grants No. EP/G054950/1, No. EP/G056803/1, No. EP/G055165/1, and No. EP/M022463/1.

[1] D. P. Higginson, J. M. McNaney, D. C. Swift, G. M. Petrov, J. Davis, J. A. Frenje, L. C. Jarrott, R. Kodama, K. L. Lancaster, A. J. Mackinnon, H. Nakamura, P. K. Patel, G. Tynan, and F. N. Beg, Production of neutrons up to 18 MeV in high-intensity, short-pulse laser matter interactions, Phys. Plasmas **18**, 100703 (2011).

[2] D. Habs, P. G. Thirolf, M. Gross, K. Allinger, J. Bin, A. Henig, D. Kiefer, W. Ma, and J. Schreiber, Introducing the fission–fusion reaction process: using a laser-accelerated Th beam to produce neutron-rich nuclei towards the N=126 waiting point of the r-process, Appl. Phys. B: Lasers Opt. **103**, 471 (2011).

[3] J. C. Fernandez and B. J. Albright, Fast ignition with laser-driven proton and ion beams, Nucl. Fusion **54**, 054006 (2014).

[4] G. H. Hartmann, O. Jakel, P. Heeg, C. P. Karger, and A. Kriessbach, Fast ignition with laser-driven proton and ion beams, Phys. Med. Biol. **44**, 1193 (1999).

[5] T. G. White, N. J. Hartley, B. Borm, B. J. B. Crowley, J. O. Harris, D. C. Hochhaus, T. Kaempfer, K. Li, P. Neumayer, L. K. Pattison, F. Pfeifer, S. Richardson, A. P. L. Robinson, I. Uschmann, and G. Gregori, Electron-Ion Equilibration in Ultrafast Heated Graphite, Phys. Rev. Lett. **112**, 145005 (2014).

[6] D. Mariscal, C. McGuffey, J. Valenzuela, M. S. Wei, J. P. Chittenden, N. Niasse, R. Presura, S. Haque, M. Wallace, A. Arias, A. Covington, H. Sawada, P. Wiewior, and F. N. Beg, Measurement of pulsed-power-driven magnetic fields via proton deflectometry, Appl. Phys. Lett. **105**, 224103 (2014).

[7] R. A. Snavely, M. H. Key, S. P. Hatchett, T. E. Cowan, M. Roth, T. W. Phillips, M. A. Stoyer, E. A. Henry, T. C. Sangster, M. S. Singh, S. C. Wilks, A. MacKinnon, A. Offenberger, D. M. Pennington, K. Yasuike, A. B. Langdon, B. F. Lasinski, J. Johnson, M. D. Perry, and E. M. Campbell, Intense High-Energy Proton Beams from Petawatt-Laser Irradiation of Solids, Phys. Rev. Lett. **85**, 2945 (2000).

[8] S. C. Wilks, A. B. Langdon, T. E. Cowan, M. Roth, M. Singh, S. Hatchett, M. H. Key, D. Pennington, A. MacKinnon, and R. A. Snavely, Energetic proton generation in ultra-intense laser-solid interactions, Phys. Plasmas **8**, 542 (2001).

[9] S. S. Bulanov, V. Y. Bychenkov, V. Chvykov, G. Kalinchenko, D. W. Litzenberg, T. Matsuoka, A. G. R. Thomas, L. Willingale, V. Yanovsky, K. Krushelnick, and A. Maksimchuk, Fast ignition with laser-driven proton and ion beams, Phys. Plasmas **17**, 043105 (2010).

[10] B. J. Albright, L. Yin, K. J. Bowers, B. M. Hegelich, K. A. Flippo, T. J. T. Kwan, and J. C. Fernández, Relativistic Buneman instability in the laser breakout afterburner, Phys. Plasmas **14**, 094502 (2007).

[11] B. M. Hegelich, I. Pomerantz, L. Yin, H. C. Wu, D. Jung, B. J. Albright, D. C. Gautier, S. Letzring, S. Palaniyappan, R. Shah, K. Allinger, R. Hörlein, J. Schreiber, D. Habs, J. Blakeney, G. Dyer, L. Fuller, E. Gaul, E. Mccary, A. R. Meadows *et al.*, Laser-driven ion acceleration from relativistically transparent nanotargets, New J. Phys. **15**, 085015 (2013).

[12] A. P. L. Robinson, M. Zepf, S. Kar, R. G. Evans, and C. Bellei, Relativistic Buneman instability in the laser breakout afterburner, New J. Phys. **10**, 013021 (2008).

[13] L. Robson, P. T. Simpson, R. J. Clarke, K. W. D. Ledingham, F. Lindau, O. Lundh, T. McCanny, P. Mora, D. Neely, C.-G. Wahlström, M. Zepf, and P. McKenna, Scaling of proton acceleration driven by petawatt-laser–plasma interactions, Nat. Phys. **3**, 58 (2007).

[14] J. Fuchs, P. Antici, E. d'Humières, E. Lefebvre, M. Borghesi, E. Brambrink, C. A. Cecchetti, M. Kaluza, V. Malka, M. Manclossi, S. Meyroneinc, P. Mora, J. Schreiber, T. Toncian, H. Pépin, and P. Audebert, Laser-driven proton scaling laws and new paths towards energy increase, Nat. Phys. **2**, 48 (2006).

[15] P. Mora, Plasma Expansion into a Vacuum, Phys. Rev. Lett. **90**, 185002 (2003).

[16] S. C. Wilks, W. L. Kruer, M. Tabak, and A. B. Langdon, Absorption of Ultra-Intense Laser Pulses, Phys. Rev. Lett. **69**, 1383 (1992).

[17] D. Mariscal, T. Ma, S. C. Wilks, A. J. Kemp, G. J. Williams, P. Michel, H. Chen, P. K. Patel, B. A. Remington, M. Bowers, L. Pelz, M. R. Hermann, W. Hsing, D. Martinez, R. Sigurdsson, M. Prantil, A. Conder, J. Lawson, M. Hamamoto, P. Di Nicola *et al.*, First demonstration of ARC-accelerated proton beams at the National Ignition Facility, Phys. Plasmas **26**, 043110 (2019).

[18] J. Kim, A. J. Kemp, S. C. Wilks, D. H. Kalantar, S. Kerr, D. Mariscal, F. N. Beg, C. McGuffey, and T. Ma, Computational modeling of proton acceleration with multi-picosecond and high energy, kilojoule, lasers, Phys. Plasmas **25**, 083109 (2018).

[19] A. J. Kemp and S. C. Wilks, Direct electron acceleration in multi-kilojoule, multi-picosecond laser pulses, Phys. Plasmas **27**, 103106 (2020).

[20] R. Mishra, F. Fiuza, and S. Glenzer, Enhanced ion acceleration in transition from opaque to transparent plasmas, New J. Phys. **20**, 043047 (2018).

[21] T. Nakamura, S. V. Bulanov, T. Z. Esirkepov, and M. Kando, High-Energy Ions from Near-Critical Density Plasmas via Magnetic Vortex Acceleration, Phys. Rev. Lett. **105**, 135002 (2010).

[22] A. Higginson, R. J. Gray, M. King, R. J. Dance, S. D. R. Williamson, N. M. H. Butler, R. Wilson, R. Capdessus, C. Armstrong, J. S. Green, S. J. Hawkes, P. Martin, W. Q. Wei, S. R. Mirfayzi, X. H. Yuan, S. Kar, M. Borghesi, R. J. Clarke, D. Neely, and P. McKenna, Near-100 MeV protons via a laser-driven transparency-enhanced hybrid acceleration scheme, Nat. Commun. **9**, 724 (2018).

[23] J. H. Bin, M. Yeung, Z. Gong, H. Y. Wang, C. Kreuzer, M. L. Zhou, M. J. V. Streeter, P. S. Foster, S. Cousens, B. Dromey, J. Meyer-ter-Vehn, M. Zepf, and J. Schreiber, Enhanced Laser-Driven Ion Acceleration by Superponderomotive Electrons Generated from Near-Critical-Density Plasma, Phys. Rev. Lett. **120**, 074801 (2018).

[24] O. Rahman, S. Tong, and Z. Sheng, Enhanced laser-driven ion acceleration by superponderomotive electrons generated from near-critical-density plasma, Phys. Plasmas **27**, 033107 (2020).

[25] J. K. Crane, G. Tietbohl, P. Arnold, E. S. Bliss, C. Boley, G. Britten, G. Brunton, W. Clark, J. W. Dawson, S. Fochs, R. Hackel, C. Haefner, J. Halpin, J. Heebner, M. Henesian, M. Hermann, J. Hernandez, V. Kanz, B. McHale, J. B. McLeod *et al.*, Progress on converting a NIF quad to eight, petawatt beams for advanced radiography, in *The Sixth International Conference on Inertial Fusion Sciences and Applications 6–11 September 2009*, San Francisco, USA, Journal of Physics: Conference Series Vol. 244 (Institute of Physics, London, 2010), p. 032003.

[26] L. J. Waxer, D. N. Maywar, J. H. Kelly, T. J. Kessler, B. E. Kruschwitz, S. J. Loucks, R. L. McCrory, D. D. Meyerhofer, S. F. B. Morse, C. Stoeckl, and J. D. Zuegel, High-energy petawatt capability for the Omega laser, Opt. Photonics News **16**(7), 30 (2005).

[27] N. Miyanaga, H. Azechi, K. A. Tanaka, T. Kanabe, T. Jitsuno, J. Kawanaka, Y. Fujimoto, R. Kodama, H. Shiraga, K. Knodo, K. Tsubakimoto, H. Habara, J. Lu, G. Xu, N. Morio, S. Matsuo, E. Miyaji, Y. Kawakami, Y. Izawa, and K. Mima, 10-kJ PW laser for the FIREX-I program, J. Phys. IV France **133**, 81 (2006).

[28] D. J. Stark, L. Y. Brian, J. Albright, W. Nystrom, and R. Bird, A detailed examination of laser-ion acceleration mechanisms in the relativistic transparency regime using tracers, Phys. Plasmas **25**, 043114 (2018).

[29] J. Peebles, M. S. Wei, A. V. Arefiev, C. McGuffey, R. B. Stephens, W. Theobald, D. Haberberger, L. C. Jarrott, A. Link, H. Chen, H. S. McLean, A. Sorokovikova, S. Krasheninnikov, and F. N. Beg, Investigation of laser pulse length and pre-plasma scale length impact on hot electron generation on OMEGA-EP, New J. Phys. **19**, 023008 (2017).

[30] T. Nakamura, S. Kato, M. Tamimoto, and T. Kato, High-energy ions from near-critical density plasmas via magnetic vortex acceleration, Phys. Plasmas **9**, 1801 (2002).

[31] A. Pukhov, Z.-M. Sheng, and J. M. ter Vehn, Particle acceleration in relativistic laser channels, Phys. Plasmas **6**, 2847 (1999).

[32] A. V. Arefiev, V. N. Khudik, A. P. L. Robinson, G. Shvets, L. Willingale, and M. Schollmeier, Beyond the ponderomotive limit: Direct laser acceleration of relativistic electrons in sub-critical plasmas, Phys. Plasmas **23**, 056704 (2016).

[33] B. S. Paradkar, M. S. Wei, T. Yabuuchi, R. B. Stephens, M. G. Haines, S. I. Krasheninnikov, and F. N. Beg, Numerical modeling of fast electron generation in the presence of preformed plasma in laser-matter interaction at relativistic intensities, Phys. Rev. E **83**, 046401 (2011).

[34] N. Iwata, K. Mima, Y. Sentoku, A. Yogo, H. Nagatomo, H. Nishimura, and H. Azechi, Fast ion acceleration in a foil plasma heated by a multi-picosecond high intensity laser, Phys. Plasmas **24**, 073111 (2017).